Polyhedron 126 (2017) 142–149

Contents lists available at ScienceDirect

Polyhedron

journal homepage: www.elsevier.com/locate/poly

Heteroleptic 1D coordination polymers: 5-Coordinated zinc(II) polymer as an efficient transesterification catalyst

Manzoor A. Wani [a], Ashish Kumar [b], Mrituanjay D. Pandey [a,*], Rampal Pandey [a,*]

[a] Department of Chemistry, Dr. Harisingh Gour Central University, Sagar 470003, MP, India
[b] Department of Chemistry, Faculty of Science, Banaras Hindu University, Varanasi 221 005, UP, India

ARTICLE INFO

Article history:
Received 12 October 2016
Accepted 7 January 2017
Available online 27 January 2017

Keywords:
1D coordination polymers
Heteroleptic
Structural studies
5-Coordination
Transesterification catalysis

ABSTRACT

The synthesis of three 1D coordination polymers (CPs), $[Zn(TPPZ)(HCCB)]_n \cdot DMF \cdot H_2O$ (**1**) $[Cd(TPPZ)(HCCB)]_n$ (**2**) and $[Co(TPPZ)(HCCB)]_n$ (**3**), based on the N,N,N-chelating κ^3-2,3,5,6-tetrakis(2-pyridyl)pyrazine (**TPPZ**) and polymerizing carboxylate ($-COO^-$) 3-(carboxy-methylamino)-4-chlorobenzoic acid (**H_3CCB**) ligands, using a solvothermal method, have been described. The CPs have been adequately characterized by satisfactory elemental analyses, FT-IR, UV–vis, emission, TGA and PXRD analysis. The structure of **1** has been verified by single crystal X-ray diffraction analysis. The structural data revealed the 5-coordinated heteroleptic polymeric framework is exclusively extended through the **H_3CCB** carboxylate group and strong N,N,N-chelating **TPPZ** ligand acts as a branch terminating site. Notably, the structure of **1** is comprised of one unit of each H_2O and DMF solvent in its crystal lattice. In contrast, **2** and **3** exclude lattice solvents, as suggested by PXRD studies, after thermal desolvation of **1**. Furthermore, **1** with 5-coordinated Zn(II) centers exhibited an efficient catalytic performance for transesterification reactions, with remarkable stability and good reusability.

1. Introduction

The design and synthesis of coordination polymers (CPs) based on mixed ligand systems have drawn a great deal of attention owing to their interdisciplinary nature, intriguing topologies and potential applications in diverse areas, including non-linear optics, magnetism, porosity, chemical sensing and catalysis [1–6]. CPs are inorganic/organometallic polymeric architectures containing metal centers linked by ligands [7]. These systems extend in one (1D), two (2D) or three dimensions (3D) through repeating units of a typical coordination complex [8,9]. Variation of the ligand plays a crucial role in the self-assembly processes and affords CPs with different structural topologies [10,11]. An extensive range of materials exhibiting a variety of architectures and functions have been prepared by adjusting the shape, flexibility, length and symmetry of the spacers [12,13]. CPs capable of displaying interesting architectures and properties can be synthesized by cautious selection of the ligand and metal ion. In this context, poly-carboxylate ligands as well as N,N-donor linkers have been extensively utilized and established their significant candidature [12,13]. Usually, neutral N-donor ligands readily coordinate to the metal centers to afford specific assemblies, however the positive charge on the metal centers is not balanced, which requires variation in the architectures. In contrast, carboxylates bring excellent diversity in the CPs as they can adopt monodentate, chelating-bidentate, bridging-bidentate, bridging-multidentate and various other binding modes with the metal centers to provide rich structural motifs, with a charge balancing capacity as an advantage over N-donor ligands [14–18]. With an objective of studying the relative coordination abilities of such systems in the same reaction environment, we attempted a solvothermal synthesis using two types of ligand systems, a bis-N,N,N-chelating ligand (**TPPZ**) and a bi-carboxylate ligand (**H_3CCB**), both possessing multiple potential donor sites in distal orientations. The simultaneous presence of these ligand systems create a competitive coordinating environment for the metal center under neutral conditions. It is well documented that designing CPs by incorporating terminal ligands can regulate the connectivity and geometry by blocking some coordination sites of the metal ions, often leading to lower dimensionality [19].

On the other hand, CPs have demonstrated fascinating catalytic properties (both homogeneous and heterogeneous) [20–24], after inspiring performances of the catalytically active metal–organic framework zeolite materials [25–28]. The most tedious job in preparative organic chemistry is the practical synthesis of complex molecules, despite applying advanced techniques which necessitates the development of catalysts being easy to prepare and

* Corresponding authors.
E-mail addresses: mrituanjaypandey@gmail.com (M.D. Pandey), rppandeysu@gmail.com (R. Pandey).

http://dx.doi.org/10.1016/j.poly.2017.01.027
0277-5387/

atom-economical [29]. In this context, due to the vital role of esters in synthetic organic chemistry, ester bond formation is an elementary and vastly studied methodology [30–37]. Pertaining to it, the synthesis of esters using the transesterification reaction is recognized as a more competent method relative to that of the dehydrative condensation of alcohols with carboxylic acids [34,36]. Herein, we report the rational coordination of the carboxylate group (in the absence of base), despite the presence of two identical bis-N, N,N-chelating donor sites in the strong **TPPZ** ligand, leading to a 1D architecture. An interesting example is the coordination of a bis-tridentate functional linker to the metal center in such a fashion that one of its N,N,N-tridentate faces coordinates in a κ^3-manner, whereas another equally potential N,N,N-tridentate site remains uncoordinated (Scheme 1, Fig. 1). In addition, **H_3CCB** bridges the 1D chain *via* two remote carboxyl groups. It depicts an unusual result in terms of coordination pattern governed by ligand competition, probably through the charge neutrality approach.

2. Experimental

2.1. Materials and methods

The common solvents and reagents like dimethylformamide (DMF) and potassium hydroxide (KOH) were procured from SD Fine Chemicals Pvt. Ltd. and used as received. Solvents were dried and distilled following standard literature procedures [38]. The ligand 2,3,5,6-tetrakis(2-pyridyl)pyrazine (**TPPZ**) was procured from Sigma Aldrich Chemical Co. Pvt. Ltd. and 3-(carboxymethylamino)-4-chlorobenzoic acid (**H_3CCB**) was prepared and purified following the procedure given below [39]. Elemental analyses were performed on an Exeter Analytical Inc. (model CE-440) CHN analyzer. IR and UV–vis spectra were acquired on FT-IR Perkin Elmer-577 and Shimadzu UV-1601 spectrometers, respectively. ^{1}H NMR (DMSO-d_6) spectra were recorded on a JEOL AL 300 FT-NMR spectrometer at an operating frequency of 300 MHz. Chemical shifts (δ) are given in parts per million (ppm) relative to tetramethylsilane (TMS, δ 0.00 ppm). Electrospray Ionization mass spectra (ESI-MS) were obtained on a Waters Q-Tof Premier Micromass HAB 213 mass spectrometer using a capillary voltage of 2.6–3.2 kV. Thermogravimetric data were obtained on a Perkin Elmer Thermal Analyzer 660 at a heating rate of 10 °C/min under a nitrogen atmosphere.

2.2. Synthetic procedures

2.2.1. Preparation of 3-(carboxymethylamino)-4-chlorobenzoic acid (*H_3CCB*)

An aqueous solution (10 mL) of 3-amino-4-chlorobenzoic acid (1.720 g, 10 mmol) was added dropwise to a solution of chloroacetic acid (1.880 g, 20.0 mmol) and KOH (1.120 g, 20.0 mmol) in water (15 mL) over half an hour and heated under reflux for 12 h. After cooling to room temperature, this gave a white precipitate which was filtered, washed with water (20 mL) and air dried. Yield: 1.605 g, 69.8%. *Anal.* Calc. for $C_9H_8NO_4Cl$: C, 47.08; H, 3.51; N, 6.10. Found: C, 46.91; H, 3.49; N, 6.00%. ^{1}H NMR (D_2O, δ ppm): 7.40 (d, 1H), 7.21 (d, 1H), 6.99 (s, 1H), 3.66 (s, 1H), 3.67 (s, 2H). IR data (KBr pellet, cm^{-1}): 3404 s, 1689 s, 1597 s, 1511 m, 1452 m, 1352 m, 1302 s, 1269 s, 1038 m, 758 s. UV–vis. (solid state, λ_{max} nm): 360, 303.

2.2.2. Preparation of [{μ_2-3-1κO-((carboxylatomethyl)amino)-4-chlorobenzoato}(N,N,N-κ^3-2,3,5,6-tetrakis(2-pyridyl)pyrazine)zinc (II)]$_n$(dimethylformamide)(water) [Zn(TPPZ)(HCCB)]$_n$·DMF·H_2O (*1*)

An aqueous solution (3 mL) of $Zn(NO_3)_2{\cdot}6H_2O$ (0.298 g, 1.0 mmol) was added to a homogenized mixture of 3-(carboxymethylamino)-4-chlorobenzoic acid (**H_3CCB**) (0.229 g, 1.0 mmol) and N,N,N-chelating κ^3-2,3,5,6-tetrakis(2-pyridyl)pyrazine (**TPPZ**)

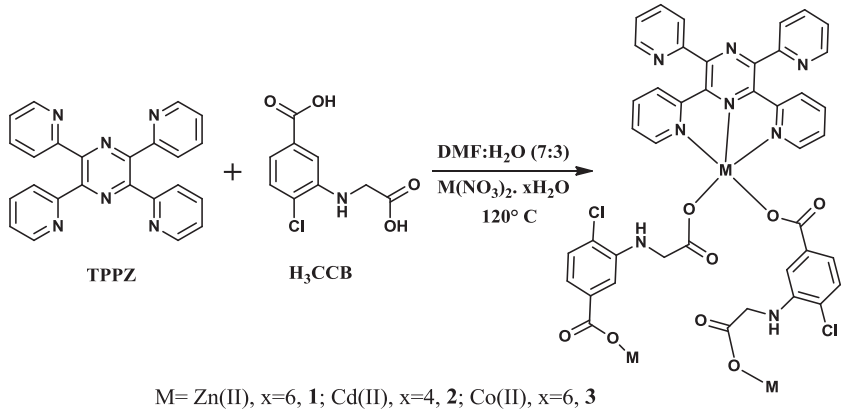

M= Zn(II), x=6, **1**; Cd(II), x=4, **2**; Co(II), x=6, **3**

Scheme 1. Preparation of heteroleptic complexes **1**–**3**.

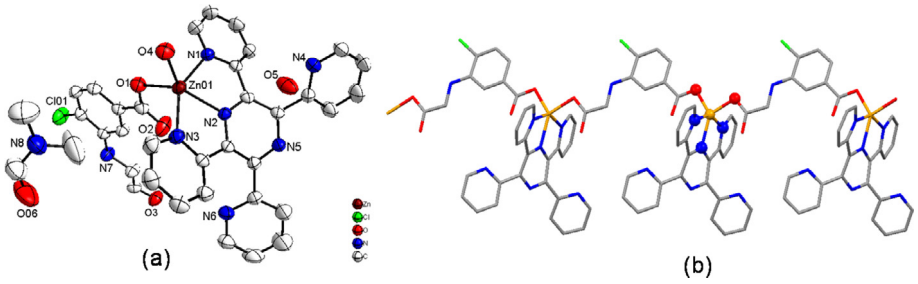

Fig. 1. (a) Structure of the asymmetric unit of **1** with the atom numbering scheme (the hydrogen atoms have been omitted for clarity). (b) 1D extended chain of **1** having the $HCCB^{2-}$ ligand bridged between the Zn(II) centers and the **TPPZ** moiety remains at one side of the chain in a *syn–syn* fashion.

(0.389 g, 1.0 mmol) in DMF (7 mL) and the ensuing reaction mixture was sonicated for 5 min. The sealed tube was immersed in an oil bath and the temperature of the bath was maintained at 120 °C for 48 h. It was slowly cooled to room temperature to afford creamy white color block shaped crystals suitable for single crystal X-ray analyses. The crystals were separated by filtration, washed several times with water and air dried. Yield: 0.334 g, 49.10%. *Anal.* Calc. for $C_{36}H_{32}ClN_8O_6Zn$: C, 55.90; H, 4.17; N, 14.49. Found: C, 55.82; H, 3.89; N, 14.28%. IR (KBr pellet, cm^{-1}): 3447 m, 3409 s, 1705 s, 1626 m, 1600 s, 1509 s, 1384 m, 1245 w, 1034 m, 758 s. ESI-MS (DMSO): *m/z* 680.0676 $[M+H]^+$ (desolvated). UV–vis (solid state, λ_{max} nm): 399, 388, 380.

2.2.3. Preparation of [{μ_2-3-1κO-((carboxylatomethyl)amino)-4-chlorobenzoato}(N,N,N-κ^3-2,3,5,6-tetrakis(2-pyridyl)pyrazine)cadmium(II)]$_n$ [Cd(TPPZ)(HCCB)]$_n$ (**2**)

This was prepared following the above procedure for **1**, except that $Cd(NO_3)_2{\cdot}4H_2O$ (0.308 g, 1 mmol) was used in place of $Zn(NO_3)_2{\cdot}6H_2O$. Compound **2** was isolated as a creamy white polycrystalline solid after cooling the reaction mixture to room temperature. Yield: 0.339 g, 46.4%. *Anal.* Calc. for $C_{33}H_{23}CdClN_7O_4$: C, 54.34; H, 3.18; N, 13.44. Found: C, 53.92; H, 2.73; N, 12.98%. IR (KBr pellet, cm^{-1}): 3407 m, 1706 s, 1598 s, 1395 m, 1299 s, 1035 m, 758 s. ESI-MS (DMSO): *m/z* 729.1423 $[M]^+$ UV–vis (solid state, λ_{max} nm): 398, 383.

2.2.4. Preparation of [{μ_2-3-1κO-((carboxylatomethyl)amino)-4-chlorobenzoato}(N,N,N-κ^3-2,3,5,6-tetrakis(2-pyridyl)pyrazine)cobalt (II)]$_n$ [Co(TPPZ)(HCCB)]$_n$ (**3**)

This was synthesized following the above procedure for **1**, except that $Co(NO_3)_2{\cdot}6H_2O$ (0.291 g, 1.0 mmol) was used in place of $Zn(NO_3)_2{\cdot}6H_2O$. Compound **3** was isolated as a pink polycrystalline solid from the reaction mixture after cooling to room temperature. Yield: 0.284 g, 42.1%. *Anal.* Calc. for $C_{33}H_{23}CoClN_7O_4$: C, 58.64; H, 3.43; N, 14.50. Found: C, 58.43; H, 3.21; N, 14.01%. IR (KBr pellet, cm^{-1}): 3404 w, 1701 s, 1597 s, 1392 m, 1298 s, 1037 m, 787 s, 750 s. ESI-MS (DMSO): *m/z* 675.0661 $[M+H]^+$ UV–vis (solid state, λ_{max} nm): 399, 386, 374.

Table 1
Crystal data and structure refinements for **1**.

	1
Identification code	shelxl-97
Empirical formula	$C_{36}H_{31}ClN_8O_6Zn$
Formula weight	772.51
T (K)	293
λ (Å)	0.710
Crystal system	monoclinic
Space group	$P2_1/c$
a (Å)	14.64
b (Å)	20.80
c (Å)	11.53
α (°)	90
β (°)	94.94
γ (°)	90
V	3499.9
Z	4
D_{calc} (g/cm^3)	1.466
Absorption coefficient (mm^{-1})	0.837
F(000)	1594.48
Crystal size (mm^3)	1 × 0.8 × 0.6
θ range for data collection	3.06–27.43
Reflections collected	7945
Independent reflections	4986
Absorption correction	T_{min} = 0.59, T_{max} = 0.71
Refinement method	Full-matrix least-squares on F^2
Goodness-of-fit (GOF) on F^2	0.984
Final *R* indices [$I > 2\sigma(I)$]	R_1 = 0.042, wR_2 = 0.085
R indices (all data)	R_1 = 0.085, wR_2 = 0.103

2.3. X-ray structure determination

Single crystal X-ray data on **1** were collected on a Rigaku R-AXIS RAPID II diffractometer at room temperature using graphite-monochromated Mo Kα radiation (*λ* = 0.71073 Å) [40,41]. The crystallographic and refinement data for **1** are summarized in Table 1. The structure was solved by direct methods (SHELXL 97, 2008) [42–44] and refined by full-matrix least squares on F^2 (SHELXL 97, 2012) [44,45]. Non-hydrogen atoms were refined with anisotropic thermal parameters. The hydrogen atoms were given a mixed treatment wherein most of the hydrogen atoms were geometrically fixed using a riding model, apart from those involved in hydrogen bonding, whose partial coordinates and isotropic atomic displacement parameters were freely refined. The computer program 'Mercury 2.3' was used for analyzing the bond lengths, weak interactions and stacking distances. The powder X-ray diffraction data was collected using an 18 kW Cu-rotating anode based Rigaku Tokyo, Japan powder diffractometer at RT and a 2*θ* range of 10–70° at a scan step of 0.02°. The XRD data were analyzed by Rietveld and Le Bail refinement techniques using the FULLPROF package.

3. Results and discussion

3.1. Syntheses and characterization

The ligand **H_3CCB** was prepared by the reaction of 3-amino-4-chlorobenzoic acid with chloroacetic acid under alkaline aqueous conditions following an earlier reported procedure [39]. The complexes **1–3** were synthesized by the reaction of metal(II) nitrates [$Zn(NO_3)_2{\cdot}6H_2O$, $Cd(NO_3)_2{\cdot}4H_2O$ and $Co(NO_3){\cdot}6H_2O$] with **H_3CCB** and **TPPZ** under controlled solvothermal conditions [M(II): **H_3CCB**:**TPPZ**; 1:1:1, 120 °C] (Scheme 1). **H_3CCB** possesses an amino-carboxylate (–NH–CH_2–COOH) and a carboxylate (–COOH) group and displays various versatile coordination modes [39]. Further, we have also attempted the synthesis using other first row transition metal ions, namely Mn^{2+}, Ni^{2+} and Cu^{2+}, under analogous conditions but remained empty handed of worthy results. Characterization of **1–3** has been achieved by elemental analyses, spectral (FT-IR, ESI-MS, electronic absorption, emission), TGA and PXRD studies. The representative 1D CP **1** has been structurally authenticated by X-ray single crystal analysis. In order to have structural information on **2–3**, their powder X-ray diffraction (PXRD) patterns have been recorded and compared with the PXRD patterns of **1** (*vide-supra*).

As shown in Scheme 1, **H_3CCB** preferably coordinates through only the κ^1-COO– mode along with concomitant coordination of **TPPZ**, resulting in infinite 1D CPs. This selective mode of bonding might be attained due to the presence of the bulky bis-N,N,N-chelating ligand (**TPPZ**) in close proximity to **H_3CCB**, leading to steric hindrance in the heteroleptic system and restricting the coordination number to five. Moreover, the charge neutrality factor of the resulting complex might also play a significant role in controlling the 5-coordination. However, the importance of the solvent nature and ratio (DMF:H_2O; 7:3) cannot be neglected in this regard [46,47].

3.2. Crystal structure of [Zn(TPPZ)(HCCB)]$_n$·DMF·H_2O (**1**)

Coordination polymer **1** crystallized in the monoclinic crystal system with the $P2_1/c$ space group (Fig. 1 and Fig. S2 in the SI). An ORTEP view along with the atom numbering scheme is shown in Fig. 1a and important crystallographic data and refinement

parameters are summarized in Table 1. The crystal structure reveals that the asymmetric unit of **1** consists of one unit each of the Zn(II) ion, bisdeprotonated ligand ($HCCB^{2-}$) and **TPPZ** ligand. However, its crystal lattice also involves one molecule each of DMF and H_2O, used as solvents in the synthesis. The immediate coordination geometry about the metal center is best described as distorted square pyramidal, comprising three N atoms from κ^3-**TPPZ** and two O atoms (κ^1-O) from two units of $\mathbf{HCCB^{2-}}$ (Fig. S3 in SI). The basal plane is formed by three N atoms of κ^3-**TPPZ** and an O atom of the amino carboxylate κ^1-COO– group of the $\mathbf{HCCB^{2-}}$ ligand. The apical position is occupied by the O atom of the aromatic κ^1-COO– group of another $\mathbf{HCCB^{2-}}$ unit at a distance of 1.997(2) Å. One should ignore the relatively short distance of the apical position since the two largest β and α angles of the basal plane are created by other four atoms, thus they are essentially involved in forming the basal plane of the distorted square pyramidal structure [48]. The Zn–O and Zn–N bond lengths vary in the range 1.997(2)–2.169(2) Å (Table S1), which lie within the range of such reported systems [39–49]. The coordination depicts that the bond distance Zn01–O1 (1.997(2) Å) is smaller than Zn01–O4 (2.037(2) Å).

The mutual difference in bond lengths is explained by tetragonality, which is measured in terms of the in-plane angular distortion described by the ratio τ [given by (β–α)/60] [48]. This ratio virtually represents the percentage of distortion in a square-pyramidal geometry. The τ value calculated here is 0.2543, which indicates the presence of a substantial distortion in the square pyramidal structure, which is further supported by significant deviations of the O–Zn–N bond angles from 90° [96.11(8)–132.94 (8)°]. Two adjacent Zn(II) ions are linked by the $\mathbf{HCCB^{2-}}$ ligand as a bridging 'spacer' to form an infinite 1D chain along the [0 1 0] direction. The **TPPZ** units are regularly present at one side of the chain, connected by three one sided N atoms (Fig. 1b). The **TPPZ** ligand is substantially twisted, the dihedral angles between the pyrazine rings and each of the pyridyl rings are found to be 24.87, 23.61, 34.52 and 33.35°. The first two values are concerned with the coordinated pyridyl rings and the latter two with non-coordinated ones. The pyrazine ring itself is puckered with the maximum atomic deviation from the best mean plane being 0.124 Å at C7. The torsion angles C6–N2–C9–C8 and N5–C7–C6–N2 are −10.174(350) and 22.891(340)° respectively, and the two C–N–C planes of the pyrazine ring exhibit a dihedral angle of 11.91°. The dihedral angle between the mean plane of the pyrazine ring and the equatorial plane defined by N3, N2, N1 and O4 atoms equals 28.57°. It is not exceptional for the pyrazine ring to be non-planar since it has been reported in the literature for related structures [50]. The responsible factors for destabilizing the planar geometry may have electronic as well as steric reasons [51].

The lattice water molecule (H5a–O5–H5b) is involved in an intermolecular hydrogen bond, O5–H5a···O3 (2.137 Å), with the oxygen atom of an adjacent aminocarboxylate moiety and an O5–H5b···N4 (2.149 Å) interaction with the nitrogen atom of a non-coordinated **TPPZ** pyridyl ring. Further, the lattice water molecule is also involved in an O5···H4–C4 (2.589 Å) interaction with the carbon atom of one of the coordinated pyridyl rings of **TPPZ** (Fig. S4; Table S2 in SI). Likewise, the lattice DMF molecule exhibits two C–H···O interactions with coordinated and non-coordinated pyridyl rings of different **TPPZ** units with distances of 2.323 and 2.594 Å, respectively (Fig. S4). Additionally, some important C–H···Z (Z = N, Cl) interactions exist [C–H···N (2.720 Å) C–H···Cl (2.779 Å)] which results in a 2D architecture, wherein the H_2O and DMF solvent molecules are alternatively stabilized (Fig. S4 in SI). An intermolecular π···π aromatic stacking interaction is exhibited between the subsequently spaced aromatic rings of $\mathbf{HCCB^{2-}}$ in a parallel displaced manner. The interlayer distance is found to be 3.507 Å and the distance between the centroids of the concerned rings is found to be 3.783 Å (Fig. S5). This type of interaction may contribute toward the stability of the polymeric architecture. The bis-N,N,N-donor groups of **TPPZ** usually adopt a bridging coordination mode, which leads to a number of transition metal coordination polymers [52]. Conversely, heteroleptic infinite CPs containing the **TPPZ** ligand showing coordination to metal centers through one end is quite scarce.

3.3. X-ray powder diffraction studies

To obtain structural information on **2** and **3**, their PXRD analyzes were performed in the limited PXRD data set from 10 to 70° (2θ) and at a scan rate of 2°.

Initially, the PXRD patterns of the synthesized complexes **2** and **3** were compared with simulated PXRD pattern of **1** obtained from X-ray single crystal data (Fig. 2). Notably, most of the PXRD profiles of **2** and **3** matched with the simulated PXRD pattern of **1**. The differences noted, especially at low 2θ values, are supposed to be attributed to the absence of lattice H_2O and DMF solvents in **2** and **3**. To get a deep insight into this, the single crystals of **1** were subjected to dynamic vacuum oven conditions by heating at 160 °C for 2 h, that in turn resulted in the loss of the transparency of the single crystals without any significant color change, which is ascribed to the desolvation of the crystal sample. To our delight, the PXRD pattern of the desolvated form of **1** matched well with those of **2** and **3** (Fig. 2). It strongly supported similar structures and coordination environments in **1**–**3**. In addition, the lack of lattice solvents (DMF and water) might be the responsible for not be able to obtain single crystals of **2** and **3**, despite several attempts under analogous reaction conditions.

3.4. Infrared and ESI-MS spectroscopic studies

The IR spectra for **1**–**3** indicated the presence of both **TPPZ** and **H_3CCB** ligands (Fig. S6a–c). In **1**, aromatic C–H stretching vibrations

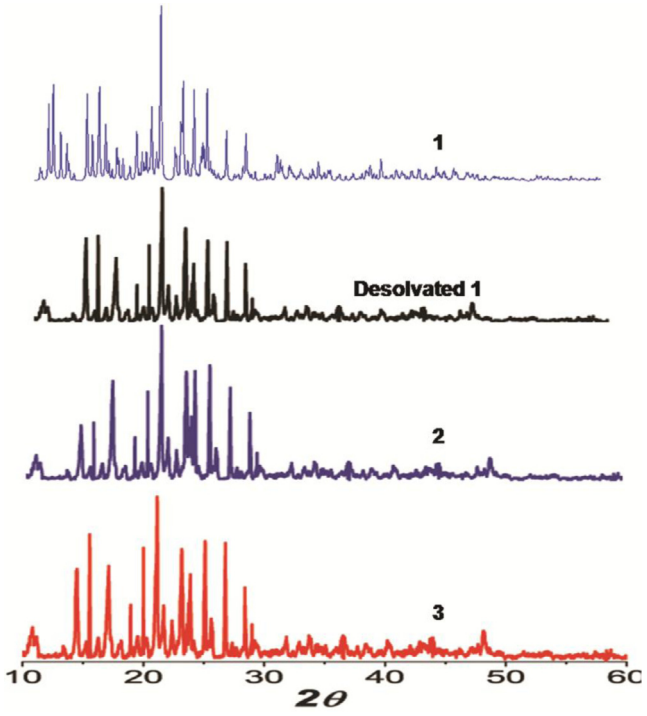

Fig. 2. Simulated PXRD patterns of **1** obtained from single crystal data (top) compared with the PXRD patterns of the desolvated form of 1 and PXRD patterns of **2** and **3**.

occur in the range 3049–2855 cm^{-1}, associated with the **TPPZ** ligand [53]. In addition, a stretching vibration at 3409 cm^{-1} due to the υ(N–H) group and two bands at 1705 and 1600 cm^{-1}, which may be attributed to the respective vibrations of υ_{asym}(C–O) and υ_{sym}(C–O) of the carboxylate groups of **H_3CCB**, are observed. A broad peak at ~3447 cm^{-1} indicates the presence of a water molecule in the lattice. In addition, a vibration at 1626 cm^{-1} is assignable to the –C=O group of dimethylformamide present in the crystal lattice. Conversely, **2** and **3** do not show any vibrations at 1626 cm^{-1}, indicating the absence of a lattice DMF molecule in their structures. Further, **2** and **3** also exhibit bands around 1705 and 1598 cm^{-1} analogous to those of **1**.

To get the better information about the stability of the CPs in the solution and the presence of lattice solvent, the ESI-MS spectra of **1**–**3** were acquired in DMSO (Fig. S7a–c). In its mass spectrum **1** displayed a molecular ion peak at *m/z* 680.0676 assignable to (Zn + **TPPZ** + **HCCB** + H)$^+$. It is noteworthy to mention here that a peak corresponding to [Zn + **TPPZ** + HCCB + DMF + H_2O]$^+$ (calc. *m/z* 781.2011) is not observed, which suggests the removal of lattice solvents from **1** in solution. Likewise, **2** and **3** also displayed molecular ion peaks at *m/z* 729.1423 (Zn + **TPPZ** + **HCCB**)$^+$ and *m/z* 675.0661 (Zn + **TPPZ** + **HCCB** + H)$^+$ in their mass spectra.

3.5. UV–vis and luminescence studies

The solid state electronic absorption spectrum of **TPPZ** displayed two bands at 301 and 359 nm assignable to the π–π* and *n*–π* transitions, respectively and **H_3CCB** displayed multiple distinct peaks in the range 230–327 nm (w) (Fig. S8 in SI). The electronic absorption spectrum of **1** exhibited several low intensity bands in the region 362–399 nm (Fig. S9a). These bands are assignable to ligand based transitions pertinent to both **H_3CCB** and **TPPZ** ligands. The absorption spectrum of **2** also followed a similar trend to that of **1**. Since both **1** and **2** are based on d^{10} systems, they do not exhibit *d*–*d* transition bands above 400 nm [54,55]. In the case of **3**, the spectrum showed several intense peaks toward high energy (357–374 nm), closely situated, and a peak at 386 nm which may be attributed to some intra-ligand π–π* transitions of the **TPPZ** ligand. The *d*–*d* transition bands responsible for the pink color of complex **3** are forbidden and thus are not observed here. Considerable red shifts are exhibited by the CPs, as well as the presence of several intra-ligand charge transfer bands pertaining to both ligand species, well supportive to the formation of the CPs.

The ligands **H_3CCB** and **TPPZ** displayed luminescence bands at 425 and 480, 510 and 528 nm, respectively (Fig. S10 in SI). The luminescence properties of the Zn(II) and Cd(II) complexes and their potential applications as new luminescent materials have drawn significant current interest [56]. The photoluminescence properties of **1**–**3** have been investigated in the solid state at room temperature. Upon excitation (λ_{ex}) at 400 nm, **1** and **2** exhibited strong emissions at 605, 539, 484 nm (**1**) and 575 (broad hump), 542, 486 nm (**2**) (Fig. S9b). In contrast, **3** displayed only two weak emissions at 597 and 530 nm (Fig. S9b). The bands at 539, 484 and 542, 486 nm in **1** and **2** are attributed to LMCT (ligand to metal charge transfer) transitions [57]. Notably, the emission intensities of **1**–**3** are quite a bit lower to those for **H_3CCB** and **TPPZ**, which may be attributed to the existence of weak interactions and promoted LMCT transitions. Moreover, significant luminescence quenching for **3** is ascribed to paramagnetic quenching, due to the presence of the Co(II) ion. The bands around ~540 nm correspond to a **TPPZ** based emission, whereas the band at ~480 nm may be attributed to the combined effect of both ligands. The absorption spectra of the heteroleptic CPs display bands centered around 360 nm that remarkably supports the coordination of the **TPPZ** group with the metal ions. It facilitates the occurrence of a ligand–metal energy transfer process and thereby reduces the overall emission intensity of the systems [58]. CPs **1**–**3** are heteroleptic thus their luminescence behavior is a combined contribution of both the ligands.

3.6. Thermal behavior

The thermal stabilities of **1**–**3** were investigated through thermogravimetric analyses in the temperature range 30–1000 °C at a heating rate of 10 °C/min under atmospheric conditions. TGA thermograms for all the complexes exhibit thermal stability of the framework (excluding lattice solvents) up to ~250 °C, whereupon decomposition of the framework starts (Fig. S9 in SI). For the TGA curve of **1**, the initial weight (wt) loss between 40 and 120 °C (3.268 wt%) is assignable to the expulsion of the lattice water molecule (Fig. S11a in SI). A subsequent two step weight loss of 8.272 and 3.278 wt% in the temperature range 120–280 °C indicates the gradual removal of the DMF molecule (9.480 wt%) present in the lattice structure and involving various weak intermolecular interactions (Fig. S4). The TGA curve shows the decomposition of the core framework starts after ~300 °C and ends at 600 °C, which is attributed to the removal of the organic linker **HCCB^{2-}** (30.488 wt%) and is consistent with the theoretically calculated mass decomposition of **HCCB^{2-}** (29.480 wt%). Further weight loss is attributed to the decomposition of the organic chelator **TPPZ** (51.077 wt%) between 600 and 860 °C, which is in good agreement with the theoretical value (50.519). The TGA curve of desolvated **1** does not show the decomposition of any lattice DMF and H_2O molecules (Fig. S11b in SI), like its single crystal form (Fig. S11a in SI). Thermal stability of the desolvated framework is found up to ~250 °C and it starts decomposing with an initial weight loss of ~24.853 wt%, ascribed to the partial removal of the **HCCB^{2-}** linker. It is consistent with the decomposition of the whole **HCCB^{2-}** except for the coordinated –COO moiety (theoretical calc. wt 26.911%), which is not decomposed below 450 °C. The subsequent weight loss between 440 and 1000 °C corresponds to the removal of the chelating **TPPZ** ligand (55.396 wt%).

Notably, the TGA curves of **2** and **3** do not show any initial weight loss corresponding to lattice solvent molecules and were found to be stable up to ~250 °C, similar to the TGA curve pattern of the desolvated form of **1** (Fig. S11c, d in SI). Initial weight losses between 250 and 400 °C are assignable to the partial removal of the linker **HCCB^{2-}** (27.258 wt%, **2**; 25.498 wt%, **3**). Consequently, the organic chelator **TPPZ** is lost between 400 and 1000 °C (52.392 wt%, **2**; 53.467 wt%, **3**), which closely resembles the TGA pattern for desolvated **1**. These observations suggest that thermal stabilities of CPs **1**–**3** are similar, however for the single crystal form of **1** the thermal weight loss starts at a lower temperature owing to the presence of lattice solvent molecules. Overall, the TGA results suggest an alike thermal decomposition pattern for complexes **1**–**3** in the temperature range 250–995 °C and thus support the analogous coordination environment.

3.7. Catalytic studies on *1*–*3*

The catalytic performance of the commercially available 4- and 5-coordinated zinc cluster $Zn_4(OCOCF_3)_6O{\cdot}CF_3CO_2H$ [59,60] in transesterification reactions motivated us to examine our 5-coordinated CPs **1**–**3** as catalysts toward transesterification reactions. The aqueous stability of **1** was probed from room temperature to 100 °C and it was observed that **1** is very poorly soluble (~10% only) in aqueous medium. Notably, **1** dissolves in dimethylsulfoxide (DMSO), which has been found to be a good choice as a solvent for transesterification reactions [61]. The identity of catalyst **1** is retained in DMSO, as is evident from its mass spectrum in the same solvent (Fig. S7a in SI). To investigate the catalytic ability of **1**, we employed transesterification reactions by varying both the ester

(**4a**–**f**) and alcohol (**5a**–**f**) reactants. However, formation of **6a** has been chosen as representative reaction for a catalytic activity discussion (Scheme 2).

Initially, **1** was dissolved in DMSO, and methyl 2-phenylacetate (**4a**) and benzyl alcohol (**5a**) were added in a 1:1 stoichiometry to the solution of **1** (as a homogeneous catalyst). The formation of the transesterification product benzyl 2-phenylacetate (**6a**) was significantly apparent over the course of ~4 h (Scheme 2). All the products (**6a**–**f**) were formed between 4 and 8 h, however in some reactions, complete consumption of the reactants required ~16 h (Scheme 3, Table 2). We have examined the best suited catalyst loading by varying the molar percentages and found an efficient catalytic activity of **1** at low catalyst loading (2 mol%). We investigated from high catalyst loading (10 mol%) to low catalyst loading (0.1 mol%) and found only a subtle change in the catalytic activity between 5 mol% (87%) and 2 mol% (86%) of **1** (Table 2). Therefore, we standardized a catalytic loading of 2 mol% in all the transesterification reactions for **6a**–**f**. Further, we successfully synthesized **6b**–**6f** using **1** as a catalyst with reasonably good yields (Scheme 3, Table 2). The ensuing transesterification products **6a**–**6f** were characterized by the NMR (^{1}H and ^{13}C) spectral technique and the ^{1}H NMR spectrum of the representative compound **6a** is given in Fig. S12. Moreover, to have a clear-cut comparison of the product formation rates, the reaction time was fixed to 4 h for every reac-

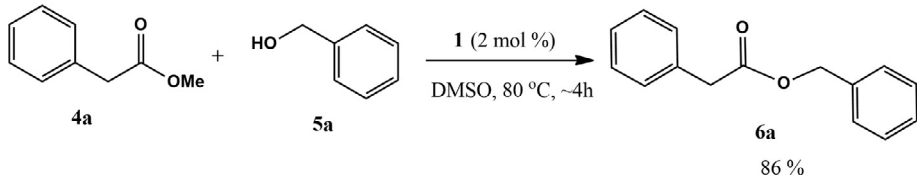

Scheme 2. Transesterification reaction employing methyl 2-phenylacetate.

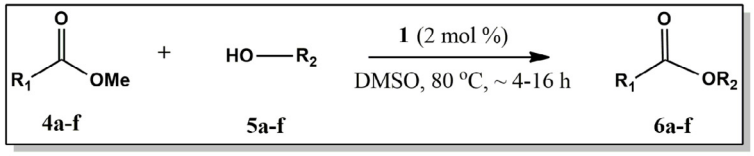

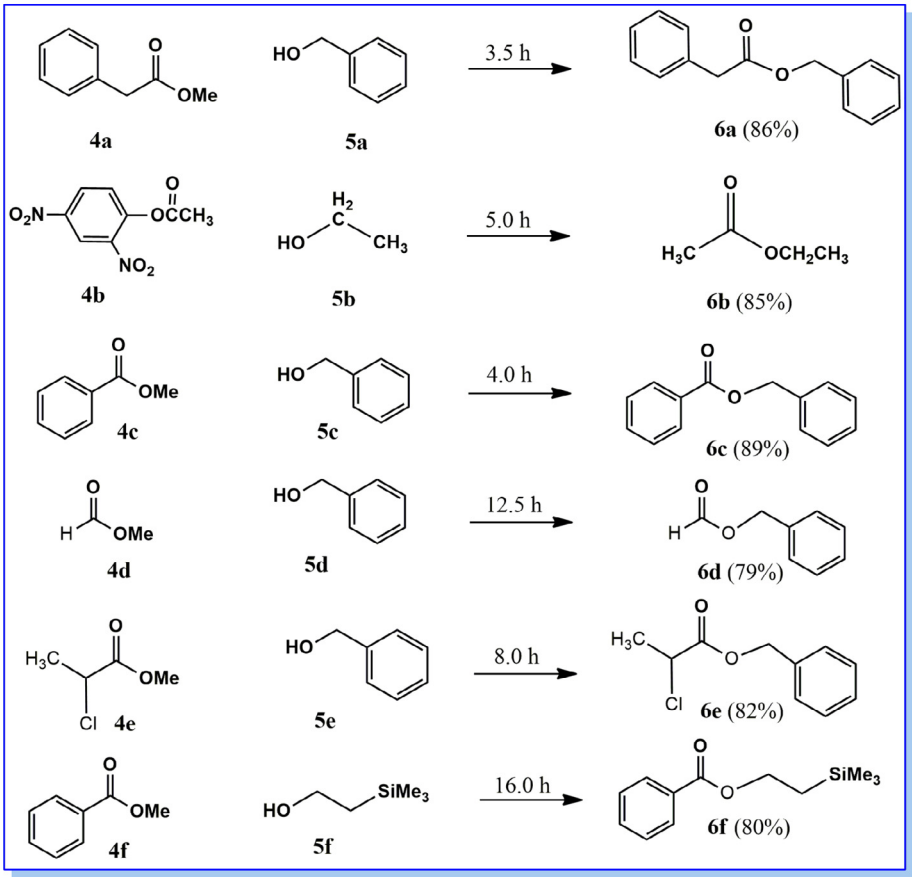

Scheme 3. Formation of transesterification products **6a**–**6f** using Zn-CP 1 as a catalyst. *The yield was calculated using the equation: Yield $(\%) = 100 \times \frac{n(\text{product})}{n(\text{reactant})}$ where n is the mole of the products and reactants.

Table 2
(1) Performance of 1 at different catalytic loading (Mol%); (2) Catalytic performances of recovered and reused 1 after several runs.

Catalytic loading of **1**	Yield (%)	Catalytic runs of recovered **1** (2 mol%)	Yield (%)
10 mol%	89	1	86
5 mol%	87	2	86
2 mol%	86	3	86
1 mol%	80	4	86
0.5 mol%	73	5	85
0.1 mol%	67	6	81

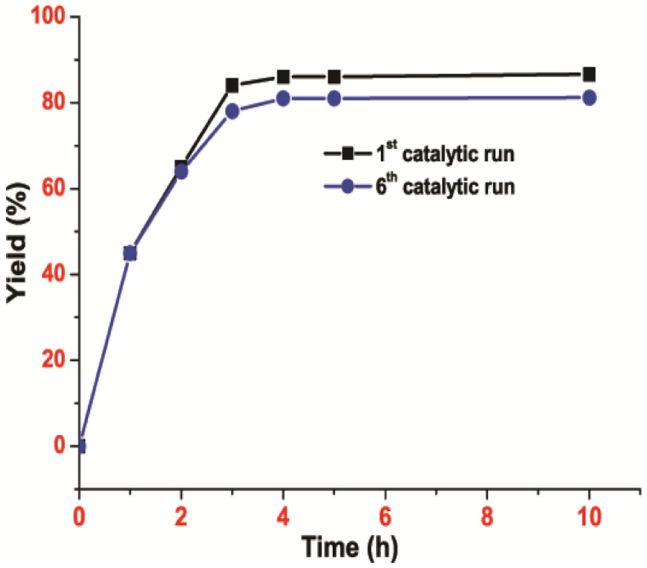

Fig. 3. Catalytic performance plot of Zn-CP **1** in the first cycle and after the sixth cycle for the trans-esterification reaction.

tion and the product yields have been compared, as listed in Table S3. Notably, the maximum conversion is observed in the case of **6c** (89%) and the minimum for **6f** (63%) after a reaction time of 4 h.

The recovery and reuse possibility of catalyst **1** was examined and notably the catalyst was recovered by extracting the organic products **6a–f** using $CH_2Cl_2/CHCl_3/C_6H_6$, leaving **1** in the reaction vessel. The catalytic efficiency of **1** was observed up to six (6) cycles and a slight decrease in the catalytic performance was found after four (4) cycles (Table 2). However, for to four cycles the catalytic efficiency was almost same (Fig. 3). The framework stability of **1** was found to be excellent, which is evident from the PXRD pattern acquired after six catalytic runs, being virtually the same as that of fresh CP **1** (Fig. S13 in SI).

The catalytic performance of **1** at the Zn^{2+} center can be considered efficient if it performs better than using the free Zn^{2+} ion as a catalyst in same solvent and under analogous conditions. With this objective, we dissolved 2 mol% of the Zn^{2+} ion [using $Zn(ClO_4)_2\cdot 6H_2O$ as the Zn^{2+} source] in DMSO and examined its catalytic performance for the transesterification reaction to yield **6a** (Scheme 4). Notably, the Zn^{2+} ion performed very poorly as compared to **1**, yielding only 52% in the first cycle, which dramatically decreased to 38% in the second cycle. It indicated very poor catalytic consistency of the free Zn^{2+} ion catalyst relative to that of **1**.

The catalytic activities of CPs **2** and **3** were also investigated under analogous conditions, wherein **3** exhibited insignificant catalytic efficiency toward the transesterification reactions. However, CP **2** showed catalytic activity toward the transesterification reactions, with quite a poor performance for the formation of **6a** (~3 times less than **1**), which suggests it acts as an ordinary catalyst for transesterification reactions. With this point of view, detailed catalytic transesterification reactions using **2** as a catalyst have been omitted. The poor catalytic performance of Cd(II) based CP **2** relative to that of **1** may be attributed to the poor labile character of the Cd(II) metal (a second-row transition metal) toward substitution reactions [62].

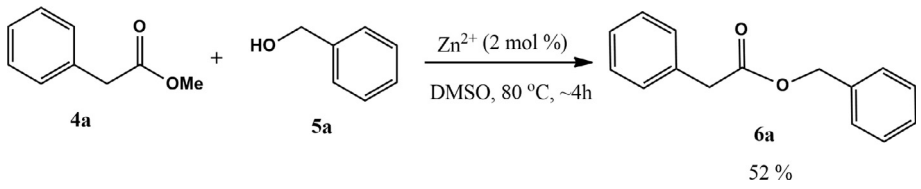

Scheme 4. Transesterification reaction employing methyl 2-phenylacetate substrate and $Zn(ClO_4)_2\cdot 6H_2O$ catalyst.

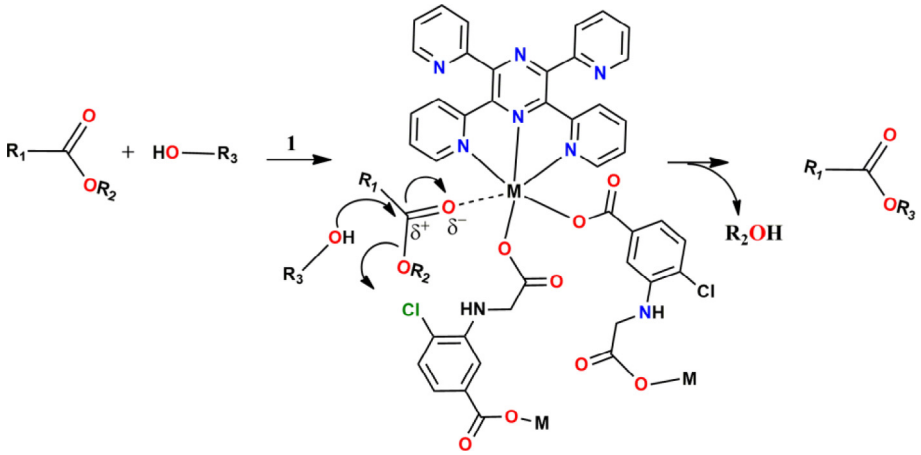

Fig. 4. Catalytic transesterification mechanism mediated by **1**.

A plausible route for the interaction of the substrates with the catalyst is shown in Fig. 4. The remarkable catalytic performance of CP **1** may be attributed to the coordinatively unsaturated labile Zn(II) center (5-coordination) which offers an open site for substrate binding (6th coordination about the Zn^{2+} center), resulting in the transesterification product [63,64].

4. Conclusion

In summary, a series of heteroleptic CPs, **1**, **2** and **3**, have been synthesized and characterized by X-ray crystallographic, spectroscopic and thermal techniques. The crystal structure of **1** reveals a distorted SPy geometry around the Zn(II) center and extends in a 1D array. The 1D architecture is achieved by the bridging **HCCB^{2-}** ligand, which exhibited a tendency to rationally coordinate through its carboxylate groups, along with the chelating κ^3-**TPPZ** ligand which binds through only one of the two identical tridentate N,N,N-donor sites. Two adjacent chains are extended parallel to each other and stabilized by $\pi\cdots\pi$ stacking interactions, H-bonding and C–H$\cdots\pi$ types of weak interactions. The Cd(II) and Co(II) CPs **2** and **3** are found to be structurally similar to **1**, as suggested by FT-IR, TGA and PXRD patterns. Thermal studies also indicated similar stabilities of **1**–**3**. The ligands and **1**–**3** exhibit significant fluorescence behavior in the solid state at room temperature, where the intensity of the **H_3CCB^{2-}** ligand is relatively stronger than the concerned polymeric complexes. Amongst **1**–**3**, CP **1** acts as a stable and reusable efficient catalyst for transesterification reactions by forming products with high time dependent yields upon low catalyst loading (2 mol%).

Acknowledgements

MAW acknowledges the UGC for financial assistance and the Department of Chemistry, Dr. Harisingh Gour Central University Sagar, (M.P.) India, for providing the research facilities. MDP acknowledges the University Grant Commission for providing financial assistance through the UGC one time Start up Grant through scheme [F.No.30-56/2014(BSR)]. RP acknowledges the Department of Science and Technology for financial assistance through the DST-Inspire Faculty scheme (IFA12-CH-66). The authors are grateful to Prof. D. S. Pandey, Department of Chemistry, Banaras Hindu University, Varanasi for helping at all the critical stages.

Appendix A. Supplementary data

Supplementary data associated with this article can be found, in the online version, at http://dx.doi.org/10.1016/j.poly.2017.01.027.

Reference

[1] N.W. Ockwig, O. Delgado-Friedrichs, M. O'Keeffe, O.M. Yaghi, Acc. Chem. Res. 38 (2005) 176.
[2] C.J. Kepert, Chem. Commun. 7 (2006) 695.
[3] K.M. Fromm, A.Y. Robin, Coord. Chem. Rev. 250 (2006) 2127.
[4] C.L. Ho, W.Y. Wong, Coord. Chem. Rev. 255 (2011) 2469.
[5] R.B. Getman, Y.S. Bae, C.E. Wilmer, R.Q. Snurr, Chem. Rev. 112 (2012) 703.
[6] J.R. Li, J. Sculley, H.C. Zhou, Chem. Rev. 112 (2012) 869.
[7] X.-M. Shi, M.-J. Fang, H.-J. Liu, X. He, M. Shao, M.-X. Li, J. Coord. Chem. 63 (2010) 3743.
[8] M. Koepf, F. Cheriouxb, J.A. Wytko, J. Weiss, Coord. Chem. Rev. 256 (2012) 2872.
[9] R. Patra, M. Hatem, H.M. Titi, I. Goldberg, Cryst. Eng. Commun. 215 (2013) 7257.
[10] H.-Q. Hao, Z.-C. Chen, W.-C. Kuang, M.-X. Peng, J. Coord. Chem. 68 (2015) 2715.
[11] P.I.M. van der List, S.J.L. Oldenbroek, E.N. Lugthart, G.A. van Albada, P. Gamez, J. G. Haasnoot, S.J. Teat, O. Roubeau, I. Mutikainen, J. Reedijk Inorg. Chim. Acta 370 (2011) 164.
[12] S. Kitagawa, R. Kitaura, S.I. Noro, Angew. Chem. Int. Ed. 43 (2004) 2334.
[13] A.E. Ion, S. Nica, A.M. Madalan, S. Shova, J. Vallejo, M. Julve, F. Lloret, M. Andruh, Inorg. Chem. 54 (2015).
[14] H.Y. Lin, J. Luan, X.L. Wang, J.W. Zhang, G.C. Liu, A.X. Tian, RSC Adv. 4 (2014) 62430.
[15] X. Zhang, L. Fan, Z. Sun, W. Zhang, D. Li, J. Dou, L. Han, Cryst. Growth Des. 13 (2013) 792.
[16] D. Niu, J. Yang, J. Guo, W.Q. Kan, S.Y. Song, P. Du, J.F. Ma, Cryst. Growth Des. 12 (2012) 2397.
[17] C.D. Si, D.C. Hu, Y. Fan, Y. Wu, X.Q. Yao, Y.X. Yang, J.C. Liu, Cryst. Growth Des. 15 (2015) 2419.
[18] Z. Zhang, J.F. Ma, Y.Y. Liu, W.Q. Kan, J. Yang, Cryst. Growth Des. 13 (2013) 4338.
[19] S. Kitagawa, S.J. Noro, T. Nakamura, Chem. Commun. 7 (2006) 701.
[20] A.L. Cheng, Y. Ma, J.Y. Zhang, E.Q. Gao, Dalton Trans. 15 (2008) 1993.
[21] J. Heo, S.Y. Kim, D. Whang, K. Kim, Angew. Chem., Int. Ed. 38 (1999) 641.
[22] A.P. Singh, A. Ali, R. Gupta, Dalton Trans. 39 (2010) 8135.
[23] A.P. Singh, G. Kumar, R. Gupta, Dalton Trans. 40 (2011) 12454.
[24] D. Bansal, S. Pandey, G. Hundal, R. Gupta, New J. Chem. 39 (2015) 9772.
[25] D.J. Lun, G.I.N. Waterhouse, S.G. Telfer, ACS Catal. 1 (2011) 1178.
[26] J. Otera, N. Dan-Oh, H. Nozaki, J. Chem. Soc., Chem. Commun. (1991) 1742.
[27] M. Hatano, K. Ishihara, Chem. Commun. 49 (2013) 1983.
[28] R. Zeng, H. Sheng, Y. Zhang, Y. Feng, Z. Chen, J. Wang, M. Chen, M. Zhu, Q. Guo, J. Org. Chem. 79 (2014) 9246.
[29] B.M. Trost, Science 254 (1991) 1471.
[30] R.C. Larock, Comprehensive Organic Transformations, 2nd ed., Wiley-VCH, New York, 1999.
[31] J. Mulzer, in: B.M. Trost, I. Fleming (Eds.), Comprehensive Organic Synthesis, 6, Pergamon Press, New York, 1992.
[32] J. Otera, Esterification, Wiley-VCH, Weinheim, 2003.
[33] R. Larock, Comprehensive Organic Transformations, 2nd ed., Wiley-VCH, New York, 1996.
[34] J. Otera, Esterification, Wiley-VCH, Weinheim, 2003.
[35] J. Otera, Chem. Rev. 93 (1993) 1449.
[36] K. Ishihara, Tetrahedron 65 (2009) 1085.
[37] J. Otera, Acc. Chem. Res. 37 (2004) 288.
[38] D.D. Perrin, W.L.F. Armango, D.R. Perrin, Purification of Laboratory Chemicals, Pergamon, Oxford, UK, 1986.
[39] R. Pandey, M. Yadav, P. Kumar, P.Z. Li, S.K. Singh, Q. Xu, D.S. Pandey, Inorg. Chim. Acta 376 (2011) 195.
[40] Rigaku, RAPID-AUTO, Rigaku Corporation, Tokyo, Japan, 1999.
[41] Rigaku, PROCESS-AUTO, Rigaku Corporation, Tokyo, Japan, 1998.
[42] G.M. Sheldrick, Acta Crystallogr., Sect. A 64 (2008) 112.
[43] H.D. Flack, Acta Crystallogr., Sect. A 39 (1983) 876.
[44] R.W.W. Hooft, L.H. Straver, A.L. Spek, J. Appl. Crystallogr. 41 (2008) 96.
[45] A.L. Spek, Private communication (2012).
[46] S.L. Cai, S.R. Zheng, Z.Z. Wen, J. Fan, W.G. Zhang, Cryst. Growth Des. 12 (2012) 3575.
[47] P.X. Yin, J. Zhang, Y.Y. Qin, J.K. Cheng, Z.J. Li, Y.G. Yao, Cryst. Eng. Commun. 13 (2011) 3536.
[48] A.W. Addison, T.N. Rao, J. Reedijk, J. Rijn, G.C. Verschoor, J. Chem. Soc., Dalton Trans. (1984) 1349.
[49] J. Tao, J.X. Shi, M.L. Tong, X.X. Zhang, X.M. Chen, Inorg. Chem. 40 (2001) 6328.
[50] J. Carranza, C. Brennen, J. Sletten, J.M. Clemente-Juan, F. Lloret, M. Julve, Inorg. Chem. 42 (2003) 8716.
[51] O.V. Shishkin, K.Y. Pichugin, L. Gorb, J. Leszczyński, J. Mol. Struct. 616 (2002) 159.
[52] C.R. Arana, H.D. Abruna, Inorg. Chem. 32 (1993) 194.
[53] K. Nakamoto, Infrared and Raman Spectra of Inorganic and Coordination Compounds, fourth ed., Wiley-Interscience, New York, 1986.
[54] F. Yuksel, Y. Chumakov, D. Luneau, Inorg. Chem. Commun. 11 (2008) 749.
[55] S.Y. Niu, Y.X. Chi, J. Jin, G.D. Yang, L. Ye, Struct. Chem. 17 (2006) 209.
[56] S.L. Zheng, J.H. Yang, X.L. Yu, X.M. Chen, W.T. Wong, Inorg. Chem. 43 (2004) 830.
[57] R.C. Evans, P. Douglas, C.J. Winscom, Coord. Chem. Rev. 250 (2006) 2093.
[58] F.P. Fugisawa, A.P. Ramos, P.C. Filho, O.A. Serra, M.E.D. Zaniquelli, J. Lumin. 132 (2012) 1116.
[59] Commercially available as ZnTAC24TM from TAKASAGO and STREM.
[60] T. Ohshima, T. Iwasaki, K. Mashima, Chem. Commun. 2006 (2006) 2711.
[61] N.R. Pedersena, P.J. Halling, L.H. Pedersen, R. Wimmer, R. Matthiesen, O.R. Veltman, FEBS Lett. 519 (2002) 181.
[62] S.J. Lippard, J.M. Berg, Principles of Bioinorganic Chemistry, University Science Books, Mill Valley, CA, 1994.
[63] A. Karmakar, M.F.C.G. da Silva, Armando J.L. Pombeiro, Dalton Trans. 43 (2014) 7795.
[64] J.S. Seo, D. Whang, H. Lee, S.I. Jun, J. Oh, Y.J. Jeon, K. Kim, Nature 404 (2000) 982.